



where  $A_{n+1}$  and  $D_n$  are the APD and diastolic interval (DI) at beats  $n+1$  and  $n$ , respectively. At the tissue scale, the diffusive coupling between cells influences the dynamics through the conduction velocity (CV) restitution relation, which describes how the depolarization wave speed depends on DI, defined here by the function  $v(D)$ . CV restitution causes the activation interval  $\bar{a}_n = A_n + D_n$  (the interval between the arrival of the  $(n-1)^{\text{th}}$  and  $n^{\text{th}}$

in the nodal region could be used to distinguish between cases where alternans is voltage driven and calcium driven. In this qualitative picture, a clear signature of the calcium-driven case would be the observation of a CaT alternans profile that is significantly steeper than the APD alternans profile or even discontinuous.

At a more quantitative level, the formation and dynamical consequences of spatial discontinuities in the CaT alternans profile remains poorly understood. From a theoretical standpoint, it would be desirable to generalize the amplitude equation approach to develop a basic understanding of calcium-driven SDA patterns for positive Ca- $V_m$  coupling.

This extension is in principle straightforward close to the alternans bifurcation, where the amplitudes of APD and CaT alternans  $A$  and  $c$ , respectively, where the amplitude of the CaT at beat  $n$  is expanded in the form  $c_n = C + (\delta c)_n$

10.1103/PhysRevE.89.052707



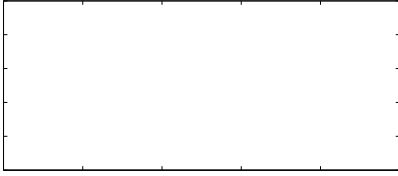
and (13) into Eqs. (6) and (6). This yields the following reduced system:

$$c_{n+1}(x) = \check{S} r c_n(x) + c_n^3(x) \check{S} a_n(x) + - \int_0^x e^{(x-\check{S}x)/\check{S}} a_n(x) dx, \quad (19)$$

$$a_{n+1}(x) = \int_0^L G(x,x) \left[ \check{S} a_n(x) \right. \\ \left. + \right.$$









Eqs. (19) and (20) and voltage-driven alternans governed by Eq. (4) [22,23] near onset. We find remarkable similarities between the dynamics, suggesting that the dynamics near onset are universal. In particular, both calcium- and voltage-driven alternans admit two classes of solutions after onset that depends on the asymmetry parameter: traveling and stationary wave patterns. For both traveling and stationary solutions, the scaling of the spatial wavelength is equivalent for calcium- and voltage-driven alternans.

In contrast, the critical onset value and velocity of traveling wave patterns of calcium-driven alternans is not precisely equivalent to the voltage-driven case. In particular, the model

solutions satisfy

$$c'(x) = \frac{\tilde{a}(x) \tilde{r} \tilde{c}(x) + c^3(x)}{\tilde{r} \tilde{c}^2(x)}. \quad (33)$$

Thus, we see that when  $\tilde{c}(x) = \tilde{r}^{-1/3}$  the denominator on the right-hand side of Eq. (33) vanishes, causing the derivative  $c'(x)$  to diverge and the profile  $c(x)$  to develop a jump discontinuity. Thus, upon formation of discontinuities, the left jumping point is given by  $\tilde{c}_s = \pm \sqrt[3]{\tilde{r}^{-1/3}}$ . To find the right jumping point we note that stationary solutions satisfy the cubic equation

$$(\tilde{r} \tilde{c}(x) - \tilde{c}^3(x)) = A(x), \quad (34)$$

where  $A(x) = \tilde{a}(x) + \int_0^x e^{(\tilde{r} \tilde{c}(x) - \tilde{c}^3(x))} \tilde{a}(x) dx$ . Since  $\tilde{a}(x)$  is smoothed by the Green's function at each iteration, the quantity  $A(x)$  remains smooth through the discontinuity in  $c(x)$ . The right jumping point  $\tilde{c}_+$  is given by the other root of Eq. (34) at  $x = x_0$ , where  $A(x_0) = (\tilde{r} \tilde{c}_s - \tilde{c}_s^3) = \pm 2(\tilde{r} \tilde{c}_s)^{3/2} / 3$ , yielding  $\tilde{c}_+ = \sqrt[3]{2(\tilde{r} \tilde{c}_s)^{3/2} / 3}$ . Finally, the total jump amplitude is given by  $|\tilde{c}_+ - \tilde{c}_s| = \sqrt[3]{\tilde{r} \tilde{c}_s}$ . In Fig. 7 we plot this theoretical prediction of  $|\tilde{c}_+ - \tilde{c}_s|$  in dashed black, noting that the agreement with numerical simulations is excellent.

We emphasize here that upon formation of discontinuities, the left and right jumping points take the values described above. We will refer to these as normal jumps as we will

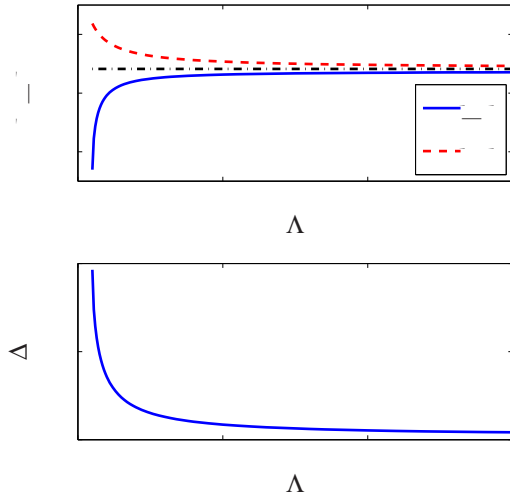
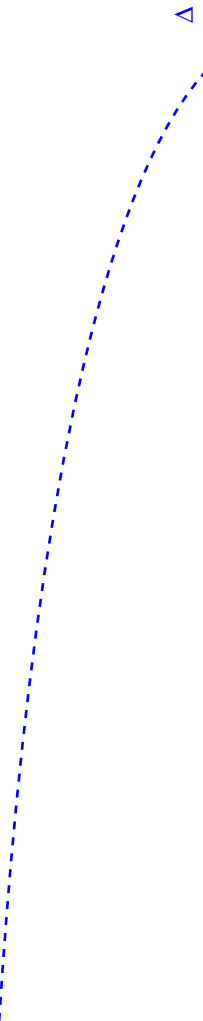
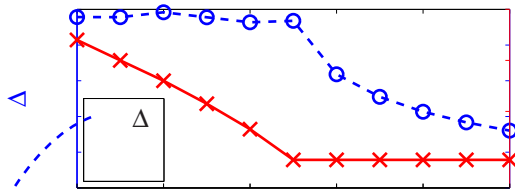
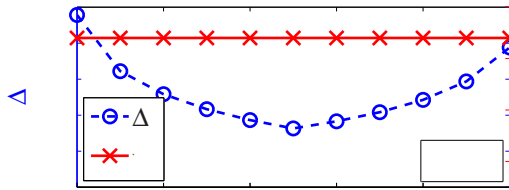
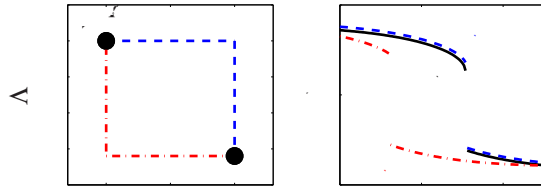


FIG. 9. (Color online) (a) Jumping points values  $|c_s|$  and  $|c_+|$  and (b) asymmetry of nodes as  $\Delta$  is increased from a steady-state profile with normal jumps with  $\tau = 1.2$  and  $\tau_0 = 10$ , plotted in solid blue and dashed red. Other parameters are  $\tau_0 = 0.3$ ,  $\tau_1 = 0$ ,  $\tau_2 = 1$ , and  $w = 0$  with  $L = 30$  and  $\Delta x = 0.005$ .

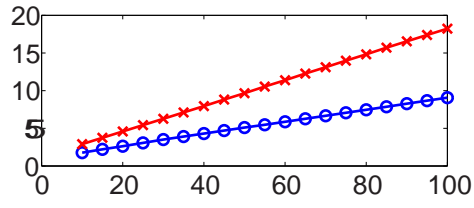
a spatial discretization of  $\Delta x = 0.005$ , and other parameters are  $\tau_0 = 0.3$ ,  $\tau_1 = 0$ ,  $\tau_2 = 1$ , and  $w = 0$ . We find that  $|c_s|$  and  $|c_+|$  approach one another in absolute value as  $\Delta$  is increased. In fact, it can be shown by studying the large limit of Eqs. (19) and (20) with  $w = 0$  that  $|c_s|$  and  $|c_+|$  approach the value  $\tau_0 \tau_2 / (\tau_0 + \tau_2)$  as  $\Delta \rightarrow \infty$ , which is denoted in dot-dashed black. This result also follows from the analysis presented in Appendix C. We see explicitly in Fig 9(b) that as  $\Delta$  increases,  $\Delta$  approaches zero. Furthermore, if we restore its original value after increasing it, the profile recovers its original shape and previous jumping point values. Finally, we note that if the symmetry of the Green's function is broken with  $w \neq 0$ , it can be shown that as  $\Delta$  is increased, the magnitude of the left jumping point  $|c_s|$  eventually surpasses the magnitude of the right jumping point  $|c_+|$ , yielding a negative value for the asymmetry  $\Delta$ .

Next, we consider the effect that decreasing  $\tau_0$  has on discontinuous solutions. Interestingly, the effect is somewhat the opposite of what was described above: the jumping points  $c_s$  and  $c_+$  remain unchanged and the node locations move towards the pacing site at  $x = 0$ . Furthermore, if  $\tau_0$  or  $\tau_2$  are restored to their original (larger) value, we find that the profile does not recover its original shape. Instead, the node remains pinned to the location closer to the pacing site and the shape of the node symmetrizes as described above. We refer to this phenomenon as unidirectional pinning.

In Fig. 10 we illustrate the phenomenon of unidirectional pinning by plotting the location of the first node as we slowly zig-zag  $\tau_0$  after obtaining a steady-state discontinuous solution at



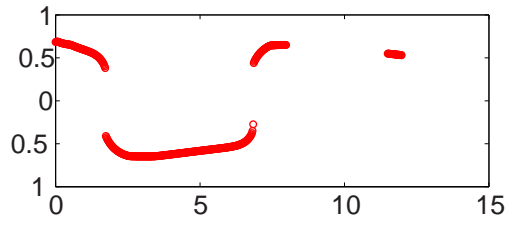




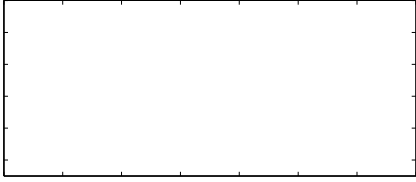
those closer to the pacing site, eventually resulting in a single





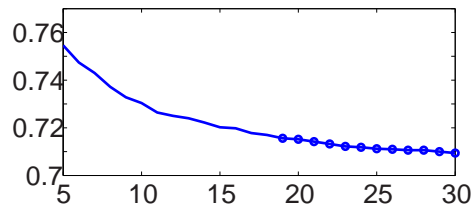














- [6] J. M. Smith, E. A. Clancy, C. R. Valeri, J. N. Ruskin, and R. J. Cohen, *Circulation* **77**, 110(1988).
- [7] A. Karma and R. F. Gilmour, *Phys. Today* **60**, 51 (2007).
- [8] G. L. Aistrup, Y. Shiferaw, S. Kapur, A. H. Kadish, and J. A. Wasserstrom, *Circ. Res.* **104**, 639(2009).
- [9] J. N. Weiss, M. Nivala, A. GarPnkel, and Z. Qu, *Circ. Res.* **108**, 98(2011).
- [10] M. A. Watanabe, F. H. Fenton, S. J. Evans, H. M. Hastings, and A. Karma, *J. Cardiovasc. Electrophysiol.* **12**, 196(2001).
- [11] D. Sato, Y. Shiferaw, A. GarPnkel, J. N. Weiss, Z. Qu, and A. Karma, *Circ. Res.* **99**, 520(2006).
- [12] B. Echebarria and A. Karma, *Eur. Phys. J. S.* **146**, 217(2007).
- [13] H. Hayashi, Y. Shiferaw, D. Sato, M. Nihei, S. F. Lin, P. S. Chen, A. GarPnkel, J. N. Weiss, and Z. Qu, *Biophys. J.* **92**, 448(2007).
- [14] S. Mironov, J. Jalife, and E. G. Tolkachev, *Circulation* **118**, 17(2008).
- [15] O. Ziv, E. Morales, Y. Song, X. Peng, K. E. Odening, A. E. Buxton, A. Karma, G. Koren, and B. R. Choi, *Physiol.* **587**, 4661(2009).
- [16] J. M. Pastore, S. D. Girouard, K. R. Laurita, F. G. Akar, and D. S. Rosenbaum, *Circulation* **99**, 1385(1999).
- [17] J. M. Pastore and D. S. Rosenbaum, *Circ. Res.* **87**, 1157(2000).
- [18] Z. Qu, A. GarPnkel, P. S. Chen, and J. N. Weiss, *Circulation* **102**, 1664(2000).
- [19] D. S. Rosenbaum, *Cardiovasc. Electrophysiol.* **2**, 207(2001).
- [20] J. J. Fox, M. L. Riccio, F. Hua, E. Bodenschatz, and R. F. Gilmour, *Circ. Res.* **90**, 289(2002).
- [21] D. Sato, Y. Shiferaw, Z. Qu, A. GarPnkel, J. N. Weiss, and A. Karma, *Biophys. J.* **92**, L33(2007).
- [22] B. Echebarria and A. Karma, *Phys. Rev. Lett.* **88**, 208101(2002).
- [23] B. Echebarria and A. Karma, *Phys. Rev. E* **76**, 051911(2007).
- [24] S. Dai and D. G. Schaeffer, *SIAM J. Appl. Math.* **69**, 704(2008).
- [25] S. Dai and D. G. Schaeffer, *ESAIM: Math. Model. Numer. Anal.* **44**, 1225(2010).
- [26] J. B. Nolasco and R. W. Dahlen, *Appl. Physiol.* **25**, 191(1968).
- [27] M. R. Guevara, G. Ward, A. Shrier, and L. Glass, *Computers in Cardiology* (IEEE Computer Society, Los Alamitos, CA, 1984), pp. 167.
- [28] M. Courtemanche, L. Glass, and J. P. Keener, *Phys. Rev. Lett.* **70**, 2182(1993).
- [29] B. Echebarria and A. Karma, *Chaos* **12**, 923(2002).
- [30] P. N. Jordan and D. J. Christini, *Cardiovasc. Electrophysiol.* **5**, 1177(2004).
- [31] D. J. Christini, M. L. Riccio, C. A. Cui, J. J. Fox, A. Karma, and R. F. Gilmour, *Phys. Rev. Lett.* **96**, 104101(2006).
- [32] T. Krogh-Madsen, A. Karma, M. L. Riccio, P. N. Jordan, D. J. Christini, and R. F. Gilmour, *Phys. Rev. E* **81**, 011915(2010).
- [33] E. Chudin, J. Goldhaber, A. GarPnkel, J. N. Weiss, and B. Kogan, *Biophys. J.* **77**, 2930(1999).
- [34] Y. Shiferaw, M. A. Watanabe, A. GarPnkel, J. N. Weiss, and A. Karma, *Biophys. J.* **85**, 3666(2003).
- [35] E. J. Pruvot, R. P. Katra, D. S. Rosenbaum, and K. R. Laurita, *Circ. Res.* **94**, 1083(2004).
- [36] E. Picht, J. DeSantiago, L. A. Blatter, and D. M. Bers, *Circ. Res.* **99**, 740(2006).
- [37] H. Bien, L. H. Lin, and E. Entchev, *Biophys. J.* **90**, 2628(2006).
- [38] J. G. Restrepo, J. N. Weiss, and A. Karma, *Biophys. J.* **95**, 3767(2008).
- [39] R. J. Rovetti, X. Cui, A. GarPnkel, J. N. Weiss, and Z. Qu, *Circ. Res.* **106**, 1582(2010).
- [40] E. Alvarez-Lacalle, I. R. Cantalapiedra, A. Penaranda, L. Hove-Madsen, and B. Echebarria, *Biophys. J.* **102**, 308a(2012).
- [41] Z. Qu, Y. Shiferaw, and J. N. Weiss, *Phys. Rev. E* **75**, 011927(2007).
- [42] Z. Jia, H. Bien, Y. Shiferaw, and E. Entchev, *Biophys. J.* **102**, 1294(2012).
- [43] D. Sato, D. M. Bers, and Y. Shiferaw, *PLoS ONE* **8**, e85365(2013).
- [44] D. M. Bers, *Excitation-Contraction Coupling and Cardiac Contractile Force* (Kluwer, Amsterdam, 2001).
- [45] J. G. Restrepo and A. Karma, *Chaos* **19**, 037115(2009).
- [46] X. Wan, M. Cutler, Z. Song, A. Karma, T. Matsuda, A. Baba, and D. S. Rosenbaum, *Heart Rhythm* **9**, 1698(2012).
- [47] Y. Shiferaw, D. Sato, and A. Karma, *Phys. Rev. E* **71**, 021903(2005).
- [48] X. Zhao, *Phys. Rev. E* **78**, 011902(2008).
- [49] Y. Shiferaw and A. Karma, *Proc. Natl. Acad. Sci. USA* **103**, 5670(2006).
- [50] S. A. Gaeta, G. Bub, G. W. Abbott, and D. J. Christini, *Circ. Res.* **105**, 335(2009).
- [51] P. S. Skardal, A. Karma, and J. G. Restrepo, *Phys. Rev. Lett.* **108**, 108103(2012).
- [52] P. A. Boyden, J. L. Pu, J. Pinto, and H. Keuroghlian, *Circ. Res.* **86**, 448(2000).
- [53] J. J. Fox, J. L. McHarg, and R. F. Gilmour, Jr., *Am. J. Physiol. Heart Circ. Physiol.* **282**, H516(2002).
- [54] B. Sandstede, in *Handbook of Dynamical Systems* (Elsevier, Amsterdam, 2002), Chap. 18, p. 983.
- [55] T. Krogh-Madsen and D. J. Christini, *Biophys. J.* **92**, 1138(2007).
- [56] T. Y. Kim, S.-J. Woo, S.-m. Hwang, J. H. Hong, and K. J. Lee, *Proc. Natl. Acad. Sci. USA* **104**, 11639(2007).
- [57] J. G. Restrepo and A. Karma, *Phys. Rev. E* **79**, 030901(R)(2009).